EuroRegio2016
June 13-15, 2016
Porto ▪ Portugal

Sound Propagation in Elliptical Ducts with Lined Walls

João M. G. S. Oliveira[1], Paulo J. S. Gil[1]

[1]IDMEC, Instituto Superior Técnico, Universidade de Lisboa, Lisboa, Portugal.
joliveira@tecnico.ulisboa.pt, p.gil@dem.ist.utl.pt

Abstract
Sound propagation in ducts with elliptical cross sections and lined walls is considered using a modal decomposition approach. The acoustic fields can be described in terms of Mathieu functions and Mathieu radial functions but the use of impedance boundary conditions leads to a coupled system of infinite algebraic equations. As a result, coupling of modes with different orders arise. Expressions for the determination of the eigenvalues and eigenfunctions are derived in the general case and an approximation is introduced for small eccentricity ($e < 0.3$) that leads to the uncoupling of the system of equations and of the modes.
For small eccentricity the eigenmodes and eigenvalues for the axial wavenumber determined were similar to those of ducts with circular cross section, which can be considered as the limiting case as the eccentricity tends to zero. The attenuation of modes is always larger in elliptical ducts when compared to circular ducts and the imaginary part of the axial wavenumber can be more than 20% higher in the examples shown. The real part of the axial wavenumber for elliptical ducts, however, can be either smaller or larger than for circular ducts, depending on the frequency and mode order.
For ducts with larger eccentricities the amount of mode coupling depends on the value of the eccentricity.

Keywords: elliptical duct.

PACS no. 43.20.Mv

1 Introduction

In this paper the acoustics of a duct with elliptic cross section, possibly carrying a uniform flow, and with lined walls will be considered. Following [1], the solution of the propagation equations in terms of Mathieu functions will be discussed. The application of the impedance boundary conditions at the duct walls lead to mode coupling, and expressions for the determination of eigenvalues and modes will be derived in the general case and in the small eccentricity approximation. Finally, a numerical example will be presented for small eccentricity. The eigenvalues and eigenfunctions obtained will be compared with those resulting from a finite element solution.

2 Sound propagation in elliptical ducts

We consider the propagation of sound in an infinite duct with elliptical cross section. The duct walls can be rigid or acoustically lined, with a locally reacting liner with impedance Z. For a sound wave of angular frequency ω the acoustic pressure can be given as a superposition of modes

$$p(x,y,z,t) = \hat{p}(x,y)e^{-i(\omega t - k_z z)} \tag{1}$$

where z is the axial coordinate and $k_z$is the axial wavenumber of the mode. $\hat{p}(x,y)$ is a solution of the transverse Helmholtz equation and the transverse wavenumber $k_\perp$ is given by the dispersion relation

$$k_\perp^2 = \left(\frac{\omega}{c}\right)^2 - k_z^2. \tag{2}$$

The transverse Helmholtz equation can be solved in elliptical coordinates (ξ,η), which are defined by:

$$\begin{cases} x = f\ \cosh\xi\cos\eta \\ y = f\sinh\xi\sin\eta \end{cases}. \tag{3}$$

with $0 \le \xi$ and $0 \le \eta < 2\pi$. For $\xi = \xi_0$, the coordinate curve is an ellipse with semi-major axis $a_e = f\cosh\xi_0$ and semi-minor axis $b_e = f\ \sinh\xi_0$. Therefore, the eccentricity of the ellipse is $e = 1/\ \cosh\xi_0$ and the focal distance is $f = a_e\, e$. As a result, the duct wall can be defined by either (f,ξ_0) or (a_e,e). Assuming that $\hat{p}(\xi,\eta) = \phi(\eta)\psi(\xi)$, the method of separation of variables leads to

$$\frac{d^2\phi(\eta)}{d\eta^2} + (a - 2\,q\ \cos 2\eta)\phi(\eta) = 0, \tag{4}$$

$$\frac{d^2\psi(\xi)}{d\xi^2} - (a - 2\,q\ \cosh 2\xi)\psi(\eta) = 0, \tag{5}$$

where a is a separation constant to be determined, and q is given by

$$q = \left(\frac{k_\perp f}{2}\right)^2 = \left(\frac{k_\perp\, a_e\, e}{2}\right)^2. \tag{6}$$

These are just the angular and radial Mathieu equations and its solutions can be given in terms of Mathieu functions. Solutions of (4) that are periodic in η, given q, exist only for certain values of a (called characteristic values) [2]. The periodic solutions are the cosine elliptic $ce_m(\eta;q)$ function (m is a non-negative integer), with a set of characteristic values given by $a = a_m(q)$; and the sine elliptic $se_n(\eta;q)$ function (n is a positive integer), with a set of characteristic values given by $a = b_n(q)$. $ce_m(\eta;q)$ is an even function of η and $se_n(\eta;q)$ is an odd function of η.
Since the set of characteristic values for the $ce_m(\eta;q)$ and $se_n(\eta;q)$ functions are different, each function is a solution of a different Mathieu angular equation (4). Therefore, given q, the periodic solution ϕ can be either $ce_m(\eta;q)$ or $se_n(\eta;q)$, but not a linear combination of both.
Solutions of (5) must be finite inside the duct. The characteristic values of (4) and (5) are the same. Following [3], the radial Mathieu functions related to the even angular functions are denoted $Je_m(\xi,q)$ and the radial Mathieu functions related to the odd angular functions will be denoted $Jo_m(\xi,q)$. The solutions of the transverse Helmholtz equation in elliptical coordinates are either even modes, $\hat{p}_\perp(\xi,\eta) = ce_m(\eta;q)\,Je_m(\xi;q)$, with $a = a_m(q)$ and $m \ge 0$, or odd modes, $\hat{p}_\perp(\xi,\eta) = se_m(\eta;q)\,Jo_m(\xi;q)$ with $a = b_m(q)$, $m > 0$. These solutions are periodic in η and finite inside the duct.

3 Boundary conditions and solutions for impedance walls

In the absence of flow the boundary condition for lined walls at the ellipse defined by $\xi = \xi_0$ is

$$\frac{\partial\hat{p}}{\partial\xi} - i\,\beta\,\Omega\sqrt{\cosh^2\xi - \cos^2\eta}\ \ \hat{p} = 0, \tag{7}$$

where $\beta = \rho c/Z$ is the specific admittance and Ω is the reduced non dimensional frequency,

$$\Omega = \frac{\omega a_e}{c}. \tag{8}$$

For even modes the solutions can be written as a linear combination of products of even Mathieu functions and even radial Mathieu functions,

$$\hat{p}(\xi,\eta) = \sum_{m=0}^{\infty} A_m \, ce_m(\eta,q)\, Je_m(\xi,q). \tag{9}$$

As shown in [1], substituting (9) in the boundary condition (7) eventually leads to an infinite homogeneous system of equations for the coefficient A_m that can be written as

$$\sum_{m=0}^{\infty} M_{nm}^{e}(\xi_0,q)\, A_m \; = 0, \tag{14}$$

where the matrix elements M_{nm}^{e}

$$M_{nm}^{e}(\xi_0,q) = N_m^e \, Je_m'(\xi_0,q)\delta_{nm} - i\,\beta\,\Omega\, I_{nm}^{e}(\xi_0,q)\, Je_m(\xi_0,q). \tag{15}$$

are written in terms of the integrals $I_{nm}^{e}\,(\xi_0,q)$ and $N_m^e\,(q)$:

$$I_{nm}^{e}(\xi_0,q) = \int_0^{2\pi} \sqrt{1-e^2\,\cos^2\eta}\;\; ce_m(\eta,q)\, ce_n(\eta,q)\, d\eta. \tag{12}$$

$$N_m^e = \int_0^{2\,\pi} ce_m^2\,(\eta,q) d\eta. \tag{13}$$

The system defined by (11) or (14) can have non trivial solutions if and only if

$$\det M_{nm}^{e}(\xi_0,q) = 0. \tag{16}$$

The roots q_r^e of (16), with $r = 1, 2, \ldots, \infty$, define the allowed values of q. Each even mode r is then given by

$$\hat{p}_r(\xi,\eta,z) = \sum_{m=0}^{\infty} A_m \, ce_m(\eta,q_r^e)\, Je_m(\xi,q_r^e)\exp[i\,k_{z_r}(q_r^e)\,z], \tag{17}$$

where the coefficients $A_{r,m}$ are the solutions of (14) with $q = q_r^e$.
Similarly, for odd modes, the solution

$$\hat{p}(\xi,\eta) = \sum_{m=0}^{\infty} B_m \, se_m(\eta,q)\, Jo_m(\xi,q), \tag{18}$$

with the boundary condition (7) leads to the matrix equation

$$\sum_{m=0}^{\infty} M_{nm}^{o}(\xi_0,q)\, B_m \; = 0, \tag{19}$$

where the matrix elements M_{nm}^{o} and the integrals $I_{nm}^{o}\,(\xi_0,q)$ and N_m^o are

$$M_{nm}^{o}(\xi_0,q) = N_m^o \, Jo_m'(\xi_0,q)\delta_{nm} - i\,\beta\,\Omega\, I_{nm}^{o}(\xi_0,q)\, Jo_m(\xi_0,q) \tag{20}$$

$$I_{nm}^{o}(\xi_0,q) = \int_0^{2\pi} \sqrt{1-e^2\,\cos^2\eta}\;\; se_m(\eta,q)\, se_n(\eta,q)\, d\eta, \tag{21}$$

$$N_m^o = \int_0^{2\,\pi} se_m^2\,(\eta,q) d\eta. \tag{22}$$

Equation (19) is a system of infinite homogeneous equations for the coefficients B_m which can have non trivial solution if and only if

$$\det M_{nm}^{o}(\xi_0,q) = 0. \tag{23}$$

The roots q_s^o of (23), with $s = 1, 2 \ldots, \infty$, define the allowed values of q. Each odd mode s is then given by

$$\hat{p}_s(\xi,\eta,z) = \sum_{m=0}^{\infty} B_m \, se_m(\eta,q_s^o)\, Je_m(\xi,q_s^o)\exp[i\,k_{z_s}(q_s^o)\,z], \tag{24}$$

where the coefficients $B_{s,m}$ are the solutions of (19) with $q = q_s^o$. Equations (17) and (24) show that the impedance boundary condition couples modes with different values of m.
Determining the roots q_r^e, q_s^o using the (truncated) determinant can be challenging because of the oscillatory nature of the integrating function in the integrals $N_m^{e,o}$ and $I_{nm}^{e,o}$. A simpler, approximate solution, valid for small eccentricity, will be derived next.

4 Approximate solution for small eccentricity

For small eccentricity, the condition $e^2 \ll 1$ applies. Using the approximation $\sqrt{1 - e^2 \cos^2\eta} \approx 1 - \frac{1}{2}e^2 \cos^2\eta + \cdots \approx 1$, the integrals I^e_{nm} and I^o_{nm}can be written as

$$I^e_{nm}(\xi_0, q) \approx \int_0^{2\pi} ce_m(\eta, q)\, ce_n(\eta, q) \quad d\eta = N^e_m(q)\delta_{nm}, \tag{25}$$

$$I^o_{nm}(\xi_0, q) \approx \int_0^{2\pi} se_m(\eta, q)\, se_n(\eta, q) \quad d\eta = N^o_m(q)\, \delta_{nm}. \tag{26}$$

where the orthogonality relations were used. Matrices M^e_{nm} and M^o_{nm} become diagonal:

$$M^e_{nm}(\xi_0, q) = N^e_m(q)[Je'_m(\xi_0, q) - i\,\beta\,\Omega\, Je_m(\xi_0, q)]\,\delta_{nm}, \tag{27}$$

$$M^o_{nm}(\xi_0, q) = N^o_m(q)[Jo'_m(\xi_0, q) - i\,\beta\,\Omega\, Jo_m(\xi_0, q)]\,\delta_{nm}, \tag{28}$$

and the coefficients A_m and B_m are all independent. Therefore, in the small eccentricity approximation there is no mode coupling.
The roots of (16) and (23) in this approximation are obtained by setting each of the diagonal terms of (27) and (28) equal to zero:

$$Je'_m(\xi_0, q) - i\,\beta\,\Omega\, Je_m(\xi_0, q), \tag{29}$$

$$Jo'_m(\xi_0, q) - i\,\beta\,\Omega\, Jo_m(\xi_0, q). \tag{30}$$

The solution no longer depends on the integrals $I^{e,o}_{nm}$ and $N^{e,o}_m$ also simplifying its evaluation.
To effectively determine the solution it is necessary to find the roots q of (29) and (30) for concrete values of the admittance β, reduced frequency Ω, and eccentricity e.

5 Example of a solution for the case of small eccentricity

In the approximation for small eccentricity, determining the roots q of (29) and (30) is equivalent, by (6) to determine the eigenvalues of the Helmholtz equation. The eigenvalues q were determined for ducts with elliptical cross-section of eccentricities $e = 0.1, 0.2, 0.3$ and several values of the reduced frequencies Ω, for both rigid walls and walls with admittance $\beta = 0.4 + 0.06\,i$. This value of the specific admittance corresponds to a specific impedance $Z/(\rho\, c) = R + i\,\chi = 2.44 - 0.37\,i$.

5.1 Comparison with numerical simulations and validation of the approximation

To validate the solutions and assess their limits of validity we compare the results with the eigenvalues obtained numerically. The numerical simulations were developed with the software package FreeFem++ [4] using finite elements to solve the eigenvalue problem defined by the transverse Helmholtz equation in cartesian coordinates. To compare all the results the problem was made non-dimensional using as normalization the semi-major axis of the elliptical duct a_e. The eigenvalues λ of the problem are,

$$\lambda \equiv K_\perp^2 = \frac{4\,q}{e^2}, \tag{30}$$

with the dimensionless transverse wavenumber $K_\perp$ defined using the semi-major axis a_e of the ellipse

$$K_\perp = k_\perp a_e. \tag{31}$$

The numerical simulations were performed for dimensionless frequency $\Omega = 10$, to better test the validity of the approximation, and admittance $\beta = 0.4 + 0.06\,i$. The mesh generation is based on the

Delaunay-Voronoi algorithm, using the number of points defined on the boundary. We increased the number of points on the boundary up to 1500 and convergence was evaluated. The number of generated triangles and vertices of the mesh depends on the eccentricity, for the same number of points on the boundary. For example, in the case $e = 0.3$ and 1500 points on the boundary the generated mesh has 382206 triangles and 191854 vertices. Each simulation takes a few minutes to run on a small laptop and, by observing the change when increasing the number of points used on the boundary from 1400 to 1500 we determined that the accuracy reached is about 6 digits.

A comparison between the eigenvalues from the approximate uncoupled solution and the eigenvalues obtained by the finite elements simulations can be found in Table 1 for dimensionless frequency $\Omega = 10$ and eccentricity $e = 0.3$. The eigenvalues are ordered by increasing real part of the approximate solution. The eigenvalues obtained numerically must be correctly matched with the right approximate value by inspecting the plot of the numerical solution. The identification becomes increasingly difficult for higher eccentricity due to mode coupling, which also change the values and the order of the modes. The relative error between the numerical an approximate modes, defined by

$$\Delta = 100 \times \frac{|\lambda_{approx} - \lambda_{num}|}{|\lambda_{num}|}, \tag{32}$$

is presented in Table 2 for increasing values of the eccentricity. As expected, the relative errors increase with eccentricity. In general the relative errors decrease with m and, for same m, with n, and are larger for even modes than for odd modes. This suggests that mode coupling is more important for even modes. For $e = 0.1$ all relative errors are below 0.25% and for $e = 0.3$ they are below 2.3%. This justifies the use of the approximate solution for these values of eccentricity. For $e = 0.5$ the relative errors are below 5% with the two exceptions of even modes (1,1) and (2,1). For many applications these relative errors are still acceptable. For $e = 0.7$ and $e = 0.9$ the relative errors increase greatly for some modes and the approximate solution is in general no longer valid. However, note that for $n = 2$ the relative errors are small, especially for odd modes.

As can be observed the error is relatively small for small to medium values of the eccentricity. Only for the highest values the relative error is considerable and other modes start to appear before the smaller ones when the eccentricity is small. The even modes seem in general to present a larger error, possibly to higher mode coupling. Also, the even and odd modes with the same orders m, n became more apart, with other modes in between (the modes not displayed before are not shown).

Table 1 – First 14 eigenvalues $\lambda = K_\perp^2$ calculated by the approximation and numerically, for $e = 0.3$ and $\Omega = 10$, ordered by increasing real part of the former.

#	m	n	parity	λ_{approx}	λ_{approx}
1	0	1	even	4.44722917 - 2.56157386 *i*	4.4409 - 2.5661 *i*
2	1	1	even	10.24112746 - 5.97511718 *i*	10.2128 - 5.9798 *i*
3	1	1	odd	10.25453668 - 6.00181520 *i*	10.2451 - 6.0033 *i*
4	2	1	even	17.42949266 - 9.15006647 *i*	17.4010 - 9.1446 *i*
5	2	1	odd	17.42974538 - 9.15048960 *i*	17.4020 - 9.1457 *i*
6	0	2	even	19.12834037 - 8.80844912 *i*	19.1027 - 8.7939 *i*
7	3	1	even	26.52391244 - 11.86384397 *i*	26.4911 - 11.8506 *i*
8	3	1	odd	26.52391637 - 11.86384884 *i*	26.4911 - 11.8507 *i*
9	1	2	even	31.42251873 - 9.50396579 *i*	31.3940 - 9.4647 *i*
10	1	2	odd	31.55681778 - 9.49133598 *i*	31.5475 - 9.4785 *i*
11	4	1	even	37.73432299 - 14.25407186 *i*	37.6986 - 14.2337 *i*
12	4	1	odd	37.73432303 - 14.25407191 *i*	37.6986 - 14.2337 *i*
13	2	2	even	47.56119203 - 9.78200307 *i*	47.5555 - 9.7547 *i*
14	2	2	odd	47.56833788 - 9.78291173 *i*	47.5480 - 9.7518 *i*

Table 2 – Relative difference $\Delta(e)$ (36) between the approximate and numerically determined modes for $\Omega = 10$ and for eccentricity $e = 0.1,0.3,0.5,0.7,0.9$.

m	n	parity	$\Delta(0.1)$	$\Delta(0.3)$	$\Delta(0.5)$	$\Delta(0.7)$	$\Delta(0.9)$
0	1	even	0.1508	1.362	3.781	7.151	8.859
1	1	even	0.2426	2.251	6.622	13.873	21.124
1	1	odd	0.0803	0.709	1.858	3.113	3.022
2	1	even	0.1475	1.667	6.370	15.806	29.906
2	1	odd	0.1433	1.294	3.558	6.479	7.076
0	2	even	0.1404	0.972	1.484	1.607	0.967
3	1	even	0.1219	1.183	4.090	12.838	31.925
3	1	odd	0.1218	1.167	3.561	7.347	9.285
1	2	even	0.1478	1.305	3.173	3.617	2.304
1	2	odd	0.0480	0.356	0.653	0.671	0.323
4	1	even	0.1021	0.970	3.054	8.543	27.840
4	1	odd	0.1021	0.972	3.014	6.797	10.115
2	2	even	0.0575	0.813	2.594	4.344	3.018
2	2	odd	0.0765	0.530	1.179	1.439	0.813

5.2 Location of wavenumbers on complex plane

Mode attenuation depends on the axial wavenumbers k_z, which were calculated using (2) and (6). The axial wavenumbers can be made dimensionless using the semi-major axis of the ellipse,

$$\mathrm{K_z} = k_z a_e. \tag{33}$$

The dimensionless axial wavenumber can be directly obtained from the dimensionless frequency and dimensionless transverse wavenumber:

$$\mathrm{K_z^2} = \Omega^2 - K_\perp^2. \tag{34}$$

The location of the dimensionless axial eigenvalues (33) in the complex plane are shown in Figure 1 for circular and elliptical ducts with lined walls, for two values of eccentricity ($e = 0.1$, left, and $e = 0.3$, right) and three different values of the reduced frequencies ($\Omega = 1, 5, 10$, from top to bottom) for the $m = 0$ even modes. Only right-running modes (with positive real part) are shown. The symmetrical solutions of (2) that lie in the third quadrant and correspond to left-running modes are not shown. For circular ducts the dimensionless wavenumbers $\widetilde{K}_z^2 = k_z R$ were determined using

$$\widetilde{\mathrm{K}}_\mathrm{z}^2 = \widetilde{\Omega}^2 - \widetilde{K}_\perp^2. \tag{35}$$

and

$$\widetilde{K}_\perp J_n'(\widetilde{K}_\perp) - i\,\beta\,\widetilde{\Omega}\,J_n(\widetilde{K}_\perp) = 0 \tag{36}$$

with a radius $R = a_e$. Note that in a circular duct the dimensionless wavenumber is $\widetilde{K}_\perp = k_\perp R$, and the reduced frequency is $\widetilde{\Omega} = \omega\, R/c$ were used.

For lined ducts, all modes are attenuated, but some lie near the real axis and are lightly attenuated, corresponding to the propagating modes in rigid ducts. Others modes lie near the imaginary axis and are strongly attenuated, corresponding to cut-off modes in rigid ducts.

This is clearly seen in Figure 1: for $\Omega = 1$ (top graphics) all modes except the first ($n = 1$) are strongly attenuated. As the frequency increases, more modes approach the real axis, and some modes are in a "transition region", moving from the vicinity of the imaginary axis to the vicinity of the real axis. The figure also shows that for the smaller eccentricity (graphics on the left), the axial

wavenumbers for the elliptical ducts are similar to those of the circular duct. For $e = 0.3$ the imaginary part of the axial wavenumbers for elliptical ducts is greater than for circular ducts, which means that axisymmetric ($m = 0$) modes in elliptical duct have higher attenuation. The real parts are also different, especially on the "transition" modes, that is, the modes that are neither near the real axis (lightly attenuated modes) nor near the imaginary axis (highly attenuated modes). However, it is difficult to identify a definite trend.

The location in the complex plane of the axial eigenvalues for the $m = 1$ modes for circular and elliptical ducts with lined walls, for two values of eccentricity ($e = 0.1$, left, and $e = 0.3$, right) and three different values of the reduced frequencies ($\Omega = 1, 5, 10$, from top to bottom) is shown in Figure 2 for even modes and in Figure 3 for odd modes. The main features are the same as in the previous case. In both cases the modes for elliptical ducts have larger imaginary part and are therefore more attenuated than the corresponding modes for circular ducts, and this effect is stronger for larger eccentricity, as would be expected. The real part of the odd modes is smaller than for even modes and tend to be smaller than for circular ducts for the two larger frequencies.

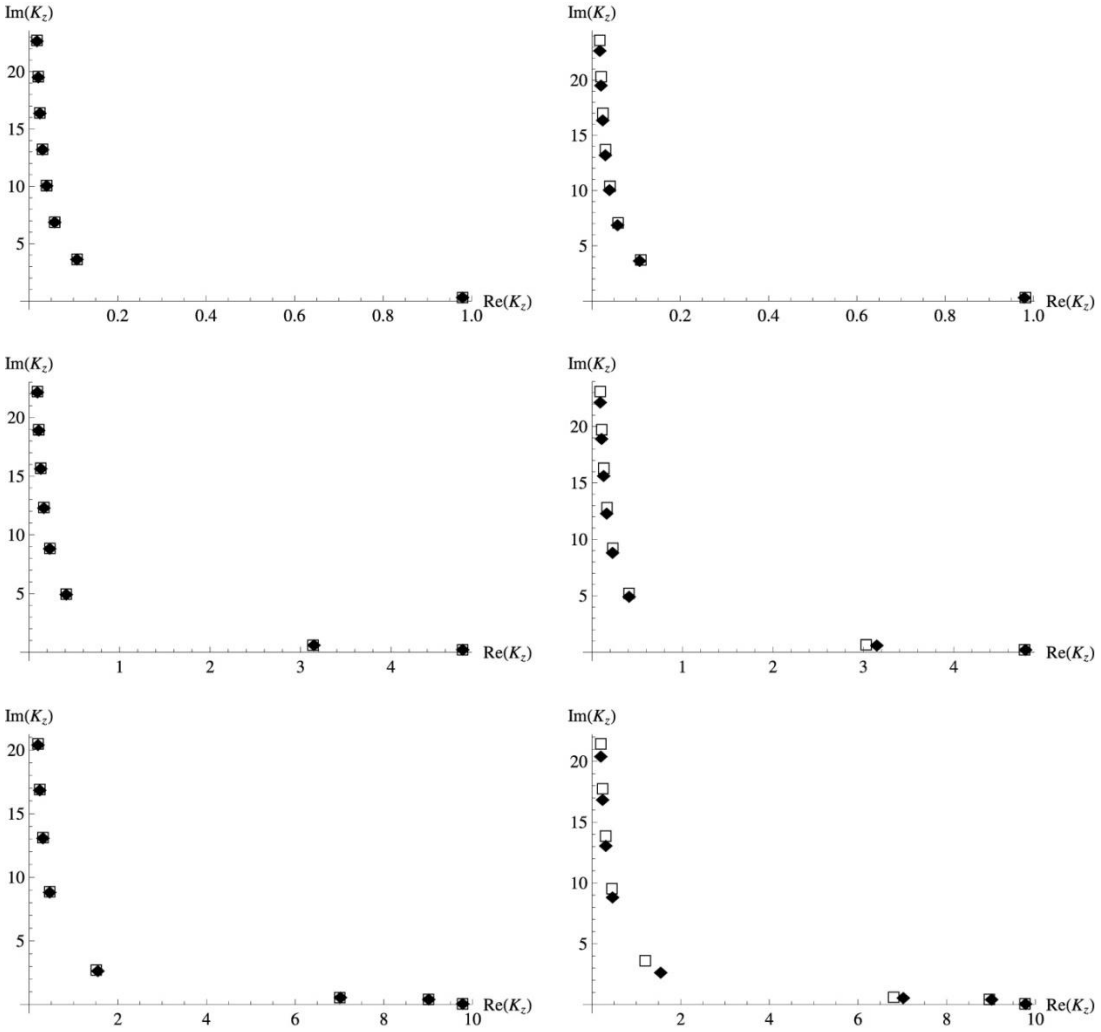

Figure 1 – Location of axial eigenvalues in complex plane for circular ducts (♦) and for even modes of elliptical ducts (□), $m = 0$ and $\Omega = 1$ (top), 5 (middle) and 10 (bottom), in the case of $e = 0.1$ (left) and $e = 0.3$ (right), for lined duct with wall admittance $\beta = 0.4 + 0.06\,i$.

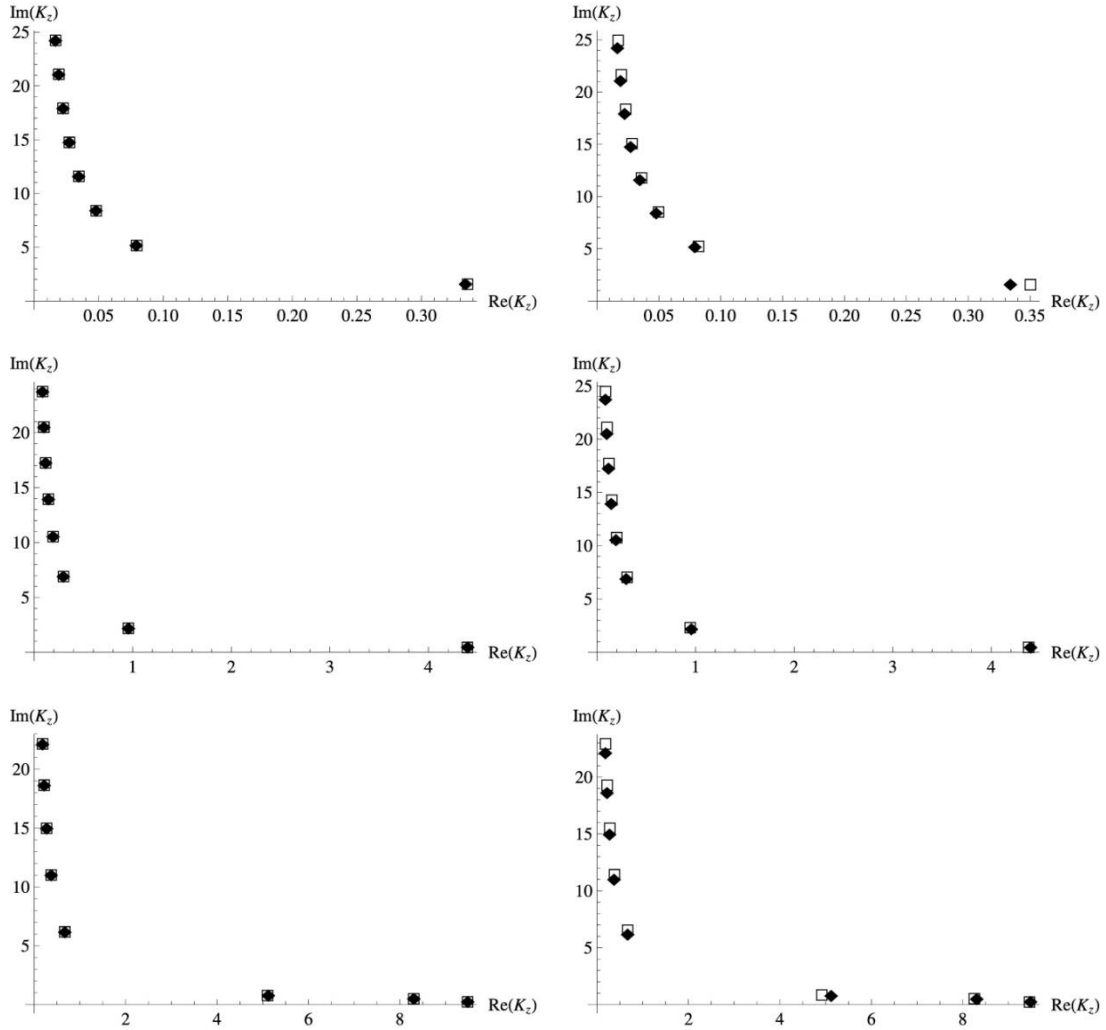

Figure 2 – Location of axial eigenvalues in complex plane for circular ducts (♦) and for even modes of elliptical ducts (□), $m = 1$ and $\Omega = 1$ (top), 5 (middle) and 10 (bottom), in the case of $e = 0.1$ (left) and $e = 0.3$ (right), for lined duct with wall admittance $\beta = 0.4 + 0.06\,i$.

6 Towards the solution for all values of the eccentricity

As stated before the solution in the case of arbitrary eccentricity is much more challenging because the matrix elements M^{e}_{nm} (15) and M^{o}_{nm} (20) are no longer diagonal and the coefficients A_m in (14) and B_m in (19)are no longer independent. The integrals (12), (21), (13), and (22) (i.e. $I^{e,o}_{nm}$ and $N^{e,o}_{m}$, respectively) must be determined in their general form for any value of the eccentricity to determine each individual term in the matrix. The system of infinite homogeneous equations for the coefficients (14) and (19) will have non-trivial solution only if the determinant of the matrix (16) and (23) are zero, respectively. Determining the roots q using the (truncated) determinant is challenging due to the oscillatory nature of the integrals. A simple numerical approach using a Computer Algebra System (Mathematica®) to help evaluate the integrals did not work, even for the case of a very small determinant as approximation, confirming the expected difficulties. To solve the problem it will be

required to acquire knowledge about the dependence of the integrals (12), (13), (21), and (22) with eccentricity, their convergence, and stability.

Preliminary calculations show that the integrals $I_{nm}^{e,o}$ can be transformed in an infinite series that can be transformed in a (infinite) normal form whose matrix coefficients depend only on a function $W_n(e)$ that depends only on the number of the column or row of the matrix and on the eccentricity (and not q). However. it is a challenge to calculate $W_n(e)$ numerically because it involves complete elliptic integrals and show as a difference of two large numbers with a small result that decreases even further with the increasing order of the series, while the large numbers increase. For example, in the case of $e = 1/2$ the function $W_n(e)$ for increasing values of n evaluates to:

$$W_8\left(\tfrac{1}{2}\right) = -2\left[42899\,\mathbf{E}\left(\tfrac{1}{2}\right) - 37344\,\mathbf{K}\left(\tfrac{1}{2}\right)\right]/45 = -3.036911 \times 10^{-6}\,, \tag{37a}$$

$$W_{12}\left(\tfrac{1}{2}\right) = -2\left[222040399\,\mathbf{E}\left(\tfrac{1}{2}\right) - 193288344\,\mathbf{K}\left(\tfrac{1}{2}\right)\right]/2145 = -8.2168412 \times 10^{-9}, \tag{37b}$$

$$W_{20}\left(\tfrac{1}{2}\right) = -2\left[1283967123044269\,\mathbf{E}\left(\tfrac{1}{2}\right) - 1117705967388744\,\mathbf{K}\left(\tfrac{1}{2}\right)\right]/6928355 = -9.8710337 \times 10^{-14}, \tag{37c}$$

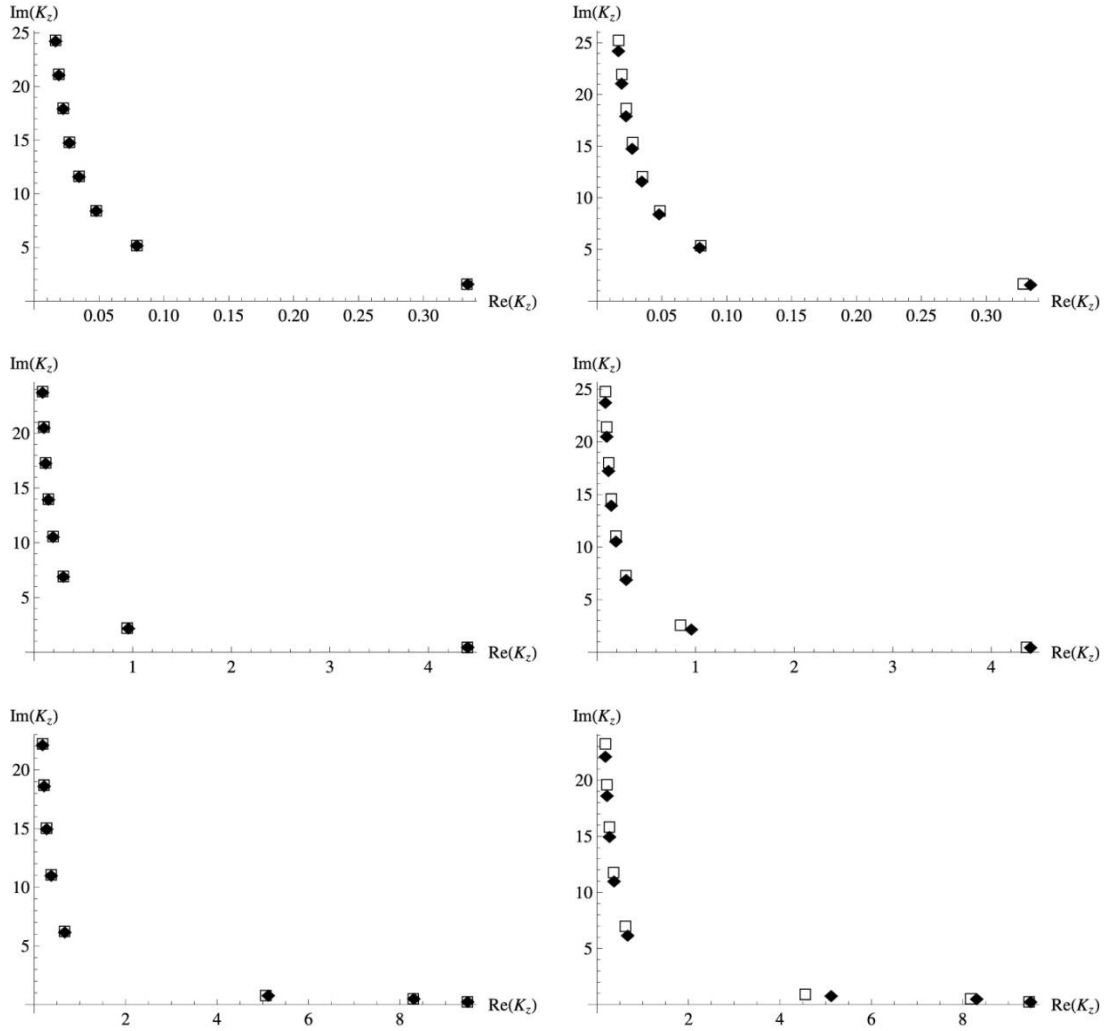

Figure 3 – Location of axial eigenvalues in complex plane for circular ducts (♦) and for odd modes of elliptical ducts (□), $m = 1$ and $\Omega = 1$ (top), 5 (middle) and 10 (bottom), in the case of $e = 0.1$ (left) and $e = 0.3$ (right), for lined duct with wall admittance $\beta = 0.4 + 0.06\,i$.

where the numerical coefficients depend on the eccentricity and $\mathbf{E}(e), \mathbf{K}(e)$ are the complete elliptic integrals of first and second kind, respectively. This situation leads rapidly to huge numerical errors. To solve the problem it will be necessary to transform the function $W_n(e)$ into something that avoids this situation. This is only part of the problem but it seems the origin of the numerical difficulties found in the attempt of solving the problem directly.

7 Conclusions

In this paper sound propagation in ducts of elliptical cross-section and lined with locally reacting liners was considered. The acoustic pressure field can be described in terms of Mathieu functions and radial Mathieu functions. The impedance boundary conditions lead to a system of an infinite number of algebraic equations, which results in the coupling of modes of different orders. The approximation for small eccentricity leads to the uncoupling of the system of equations and of the modes. Comparison with FEM simulations validates this approximation for $e \leq 0.3$ and shows that for $e \leq 0.5$ results are still acceptable. For higher values of the eccentricity the results from the approximation give large relative errors for some modes. Results for odd modes are in general better than for even modes, suggesting that mode coupling is more important for the latter

The eigenmodes and eigenvalues for the axial wavenumber that were determined for the case of small eccentricity were similar to those of ducts with circular cross-section, which can be considered as the limiting case as $e \to 0$. The attenuation of modes is always larger in elliptical ducts when compared to circular ducts and $Im(K_z)$ can be more than 20% higher in the examples shown. The real part of the axial wavenumber K_z for elliptical ducts, however, can be either smaller or larger than for circular ducts, depending on the frequency and mode order

The cut-off frequency of rigid ducts was found to be an important parameter for the behaviour of the modes, at least for the example shown, in which a small admittance was used. The usual classification in evanescent and propagating modes is no longer valid. However, modes can be classified as: (i) strongly attenuated, for frequencies much smaller than the cut-off frequency of the mode; (ii) lightly attenuated, or ``propagating", modes, for frequencies much larger than the cut-off frequency; and (iii) transition modes, for frequencies comparable to the cut-off frequency. This classification has been used before for lined circular ducts, and it remains valid for lined elliptical ducts of small eccentricity.

A difficulty in dealing with the general case of arbitrary eccentricity was identified that can suggest a line of action to find the general solution.

Acknowledgements

This work was supported by FCT, through IDMEC, under LAETA, project UID/EMS/50022/2013.

References

[1] Oliveira, J. M. G. S.; Gil, P. J. S. Sound propagation in acoustically lined elliptical ducts. *Journal of Sound and Vibration*, Vol 333, 2014, pp 3743-3758.

[2] McLachlan, N. *Theory and application of Mathieu functions*, Oxford University Press, 1947.

[3] Gutiérrez-Veja, J. C.; Rodrígues-Dagnino R. M.; Neneses-Nava, M. A.; Chávez-Cerda, S. Mathieu functions, a visual approach. *American Journal of Physics*, Vol 71, 2003, pp 233-242.

[4] Hecht, F. New development in freefem++, *Journal of Numerical Mathematics*, Vol. 20 (3-4), 2012, pp 251-265.